ACS Catalysis

Research Article

pubs.acs.org/acscatalysis

Reduction Characteristics of Ceria under Ethanol Steam Reforming Conditions: Effect of the Particle Size

I. Ilgaz Soykal,[†] Hyuntae Sohn,[†] Deepika Singh,[†] Jeffrey T. Miller,[‡] and Umit S. Ozkan*,[†]

[†]Department of Chemical and Biomolecular Engineering, The Ohio State University, 140 W. 19th Avenue, Columbus, Ohio 43210, United States

[‡]Chemical Sciences and Engineering Division, Argonne National Laboratory, 9700 S. Cass Ave, Argonne, Illinois 60439, United States

ABSTRACT: Reducibility of ceria under steam reforming conditions and the effect of particle size on its reducibility was examined using two ceria samples with distinctly different mean particle sizes (3.5 nm versus 120 nm), but with similar polyhedral morphologies. The degree of reduction from Ce^{4+} to Ce^{3+} was characterized by temperature programmed reduction (TPR) and *in situ* X-ray absorption near edge structure spectroscopy (XANES) where the nanopolyhedra were observed to reduce much more readily compared to the larger particle-size sample. There was also significant reduction of the nanopolyhedra under ethanol steam reforming conditions. Ceria nanopolyhedra exhibited significantly more Ce^{3+} sites which contributed to a lower occurrence of surface acidic sites. The acidic/basic sites were probed by probe molecules such as pyridine and CO_2 through *in situ* diffuse reflectance infrared spectroscopy (DRIFTS). The particle size also showed major differences in the steam reforming activity of ceria, with nanopolyhedra with a 3.5-nm mean particle size exhibiting significantly higher carbon cleavage and ethanol dehydration activity than its counterpart of 120 nm mean particle size.

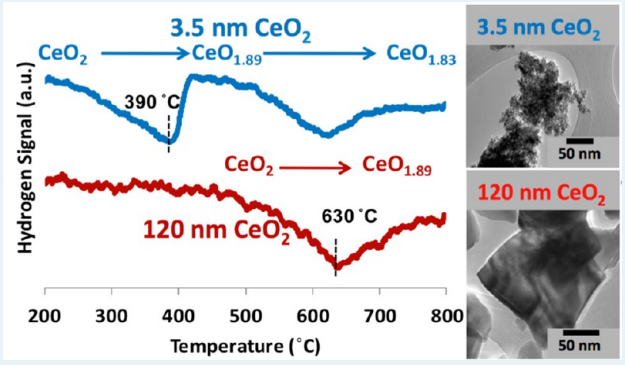

KEYWORDS: *ceria, cerium, XANES, ethanol, solvothermal, nanoparticles*

1. INTRODUCTION

There has been widespread interest in CeO_2 due to its high thermal stability and electronic properties[1,2] for applications as a catalyst support, as well as a stand-alone catalyst in several reactions such as CO oxidation,[3] oxidative dehydrogenation,[4] and steam reforming.[5−7] It is well established that Ce has the ability to undergo rapid transformations between Ce^{4+} and Ce^{3+} states under oxidizing and reducing environments. The ability to move back and forth between oxidation states imparts ceria with catalytic activity for reactions with redox cycles.

Ceria has been shown to be an effective support in ethanol steam reforming reactions when used with noble metals such as Pt and Rh,[8−11] or with transition metals such as Ni, Cu, and Co[12−21] and has been widely investigated, including in studies from our laboratories.[6,7,14,15,22−28] In these studies, catalysts supported on ceria were found to have significantly higher relative basicity[27] and higher oxygen mobility compared to those supported on other oxides, such as Al_2O_3, TiO_2, and ZrO_2.[14] Changing the oxygen mobility in the ceria lattice by the addition of a divalent cation such as Ca was also demonstrated.[15] In our more recent studies, the role of crystal morphology as well as particle size of the ceria support was examined over Co-based catalysts.[6,7]

Although the effect of the ceria support properties, i.e., surface acidity, morphology, particle size, and oxygen mobility, has been clearly demonstrated in ethanol steam reforming, the presence of a metal or metal oxide (e.g., Co, CoO_x) has not allowed elucidating the role of the ceria support in the ethanol steam reforming reaction scheme. In order to isolate the role of ceria in such catalytic systems, it also needs to be investigated in the absence of additional metals and/or metal oxides.

The properties of ceria have been reviewed by Trovarelli from a broader perspective for catalysis applications.[1] Previous research conducted on bare ceria has shown significant ethanol reforming activity for different ceria morphologies,[6] where nanocube morphologies showed an abundance of the (110) crystal planes, which were more active for steam reforming compared to nanorods.[4,5,29,30] Resasco and co-workers investigated the behavior of ceria containing mixed oxides and most importantly the correlation between support reduction and steam reforming activity.[31−33] The Flytzani-Stephanopoulos group had significant contributions to understanding the effect of ceria morphology on many reactions, including the water gas shift reaction.[34−37] Zhou and Huebner investigated the effect of ceria particle size and reported that the oxygen vacancies increased by 2 orders of magnitude when particle size was reduced from 60 to 4 nm.[38] Laachir et al. quantified ceria reduction with respect to particle size which

Received: October 10, 2013
Revised: January 2, 2014
Published: January 6, 2014

was controlled by increasing the calcination temperature.[39] Nolan et al. focused on density functional theory calculations to improve the understanding of the oxygen vacancy formation, which was reported to increase metallic dispersion.[40,41]

Ceria particle size has shown a significant effect on surface chemistry in multiple reactions, but its effect on steam reforming warrants further investigation. Hence, in this paper, we present the results regarding the effect of ceria reducibility where a highly reducible nanopolyhedra catalyst with 3.5-nm particle size was synthesized and compared with 120-nm commercial ceria particles. Structural characterization was performed by X-ray diffraction (XRD), surface area analysis, and high resolution transmission electron microscopy (HR-TEM). The extent of reduction is investigated by quantitative temperature programmed reduction (TPR), and in situ X-ray near edge fine structure (XANES). The effect of ceria reduction on surface species was investigated in terms of surface acidity and basicity with diffuse reflectance infrared spectroscopy (DRIFTS) using pyridine and CO_2 as probe molecules. Preoxidized and prereduced ceria were evaluated for their performance and activity for ethanol and ethylene steam reforming with steady state reaction experiments along with Co impregnated Co/CeO_2 catalysts in order to provide a baseline for ceria activity. The effect of cobalt on steam reforming over ceria has been investigated in our previous work and was not a focus in this paper.

2. EXPERIMENTAL SECTION

2.1. Catalyst Preparation. Ceria nanopolyhedra (CeO_2-NP) were prepared via the solvothermal[42] method where 2 g of ceriumisopropoxide precursor (Alfa Aesar, Ce 37−45%) is mixed with 20 mL of benzyl alcohol (Alfa Aesar, 98%). The mixture was rigorously stirred until the ceriumisopropoxide was dissolved. A total of 10 mL of benzyl alcohol was added, and the resulting brownish solution was transferred to a 50-mL stainless steel autoclave, which was heated at 200 °C for 24 h in an oven. Following the precipitation, the autoclave was cooled down to room temperature and the suspension was filtered. The remaining solids were washed with water and dried overnight at 90 °C. The dried sample was tested as uncalcined ceria. The solids were then calcined at 450 °C for 3 h under air to yield ceria nanopolyhedra with a light yellow color (denoted as CeO_2-NP). Commercial ceria with a particle size in the 0.1 μm range (denoted as CeO_2-MP) was prepared by calcining Sigma Aldrich 99.999% <5 μm CeO_2 at 450 °C for 3 h in the air.

Ten percent (by weight, metallic) cobalt was impregnated on both samples via the incipient wetness impregnation method with $Co(NO_3)_2$ (Aldrich, 99.999%) dissolved in 200 proof ethanol (Decon Labs) and applied onto the ceria in six consecutive steps by drying the impregnated catalyst at 110 °C overnight in between each step to improve the homogeneity of the resulting catalyst. Following the final impregnation and drying step, the catalyst was calcined at 450 °C for 3 h under air flow.

2.2. Catalyst Characterization. *2.2.1. Surface Area, Pore Volume, and X-Ray Diffraction (XRD).* BET surface area and pore volume were measured by a Micromeritics ASAP 2020 accelerated surface area analyzer and porosimetry instrument, using nitrogen adsorption and desorption isotherms collected at liquid N_2 temperature. BJH pore size distribution was determined by the desorption branch of the isotherm. Before measurement, the catalyst was degassed for 12 h at 130 °C under a vacuum better than 2 μm Hg. A Rigaku X-ray diffractometer (X-ray source: Cu Kα radiation, λ = 1.5418 Å) operated at 40 kV and 25 mA was used to collect the diffraction patterns of the samples.

2.2.2. Transmission Electron Microscopy (TEM). A Phillips Tecnai F20 instrument equipped with a field emission gun operated at 200 kV was used for obtaining the CeO_2-MP and CeO_2-NP TEM images. Samples were suspended in 200 proof ethanol (Decon Labs) and were sonicated for 10 min. The resulting suspension was deposited on a Tedpella, Inc. 200 mesh copper grid coated with lacey carbon. ImageJ processing software is used for the analysis of the TEM digital micrographs.

2.2.3. Temperature-Programmed Reduction (TPR). The reduction of ceria samples was characterized by TPR. The quantification was done using CuO as a reference. A total of 50 mg of CuO was packed in a 1/4″ OD quartz tube and loaded into a Carbolite MTF 10/15/130 furnace. The sample was reduced under 30 cc/min 5%H_2/He with a temperature ramp of 10 °C/min. The effluent during reduction was monitored via a residual gas analyzer (MKS-Cirrus II) operated in scanning ion mode. A 100× multiplier detector was used to monitor the signals for m/z = 2, 4, 17, 18. The peak area for m/z = 2 was calculated and used as a standard for quantification of hydrogen used during reduction. Fifty milligrams of CeO_2-MP and CeO_2-NP samples was reduced similarly, and the extent of reduction was quantified using copper oxide as a standard.

2.2.4. X-Ray Adsorption near Edge Spectroscopy. Catalyst samples were investigated in situ under ethanol steam reforming conditions in terms of their cerium coordination environment using the controlled-atmosphere X-ray absorption fine structure (XAFS) technique. The spectra were collected for the Ce LIII-edge at the bending magnet beamline (5BM-D) of the Dow−Northwestern−DuPont Collaborative Access Team (DND-CAT) of the Advanced Photon Source, Argonne National Laboratories. The measurements were made in transmission mode with the Si(111) monochromator detuned by 30% to eliminate the higher order harmonics in the beam. CeO_2 samples were mixed with SiO_2 at a ratio of 1:8 and finely ground (<150 mesh) to obtain a homogeneous mixture. Approximately 6 mg of the mixture was then pelletized using a 6-mm polished steel die and placed inside a 5-cm-long quartz tube (6.5 mm ID) and supported with quartz wool plugs. The sample was then centered in a 45 × 2 cm controlled-atmosphere XAFS chamber that was fitted with Kapton® windows. The XAFS reactor setup allowed continuous flow of the reactants as well as the isolation of the catalyst sample.

The preoxidized catalyst was heated to 400 °C and kept under He for the initial spectrum collection. Following that, it was kept under the ethanol steam reforming mixture of 0.3% ethanol and 3% water. In situ XANES data on the sample was collected at 400, 450, and 500 °C. At each temperature step, the catalyst was kept on stream for 60 min and the XANES spectra were collected in the presence of the reaction mixture. The prereduced sample was reduced in situ at 400 °C with 3.6% H_2 in the XAFS reactor for the initial spectrum. The gas phase was flushed with He for 1 h, and the in situ XANES data were collected following the pretreatment. XANES spectra were obtained by linear combination fitting of CeO_2 (Sigma Aldrich, <25 nm particle size nanopowder) and Cerium nitrate hexahydrate standards for the Ce^{4+} and Ce^{3+} phases, respectively.

2.2.5. Diffuse Reflectance Infrared Spectroscopy (DRIFTS). A Thermo NICOLET 6700 FTIR spectrometer equipped with a liquid-nitrogen-cooled MCT detector and a KBr beam splitter was used for *in situ* diffuse reflectance Fourier transform infrared spectroscopy (DRIFTS). The samples were loaded into a Praying Mantis diffuse reflectance controlled atmosphere chamber with ZnSe windows and were pretreated at 400 °C under 30 cm^3/min He flow. Samples underwent additional treatment with reduction for 1 h in 5% H_2/He (30 ccm) at the same temperature and purging with He (30 ccm) for 1 h at 450 °C. Following the pretreatment step, temperature was lowered to 400 °C under 5% H_2 balance He flow, and the background spectra were collected every 50 °C, during cooling. CO_2 and pyridine were used separately as probes for basic and acidic sites, respectively. At room temperature, the selected probe molecule was introduced with CO_2 in the gas flow and pyridine through bubbling He through liquid pyridine. Following 1 h of adsorption, the sample was flushed 1 h with He to remove the gas phase. Spectra were collected during the temperature ramp at every 50 °C step up to 400 °C.

2.3. Steady-State Catalytic Activity Testing. The steady-state ethanol steam reforming activity data were collected in the 350−450 °C range using a fixed bed flow reactor system, which consisted of a feed system capable of delivering reactant mixtures of desired flow rate

dx.doi.org/10.1021/cs400908h | ACS Catal. 2014, 4, 585−592

and composition, a 4-mm-ID quartz reactor with a quartz frit, and an online gas chromatograph. For each run, a 20−150 mg batch of the CeO_2 was packed inside the reactor. The reactor was placed inside a resistively heated furnace (Carbolite, MTF 10/15/130), and the temperature was controlled by an Omega CSC232 PID temperature controller. Helium was used as the carrier gas, and the reactants were introduced to the helium stream using a heated evaporator-syringe pump assembly. The reactants, water and ethanol, at a 10-to-1 molar ratio, were fed to an evaporator maintained at 230 °C, using pulse-free syringe pumps (Cole-Parmer). The gas lines in contact with the reactant gas stream were heated to 130 °C to prevent condensation. The steady-state reaction experiments were run in the kinetically controlled regime by maintaining the reaction conditions away from equilibrium at all temperatures. The reaction experiments were conducted with a feed stream concentration of 1.7% ethanol and 17% water balance helium. The weight hour space velocities (WHSV) ranged between 0.19 and 2.88g EtOH $(g\ cat)^{-1}\ h^{-1}$ and were varied to allow for equal surface area comparisons. Prereduced catalyst samples were subjected to the reduction pretreatments at 400 °C as described earlier in the section.

The reported reactant conversion and product yield values are representative of the catalytic activity after a steady state was reached at each temperature. Ethanol conversion, hydrogen yield, and selectivity of carbon containing species are defined as follows:

$$\text{ethanol conversion (\%)} = \frac{\text{moles of ethanol converted}}{\text{moles of ethanol fed}} \times 100$$

$$H_2\ \text{yield (\%)} = \frac{\text{moles of } H_2 \text{ produced}}{6 \times (\text{moles of ethanol fed})} \times 100$$

$$\text{yield of C-containing product } i\ (\%) = \frac{(\#\text{C atoms}) \times (\text{moles of } i \text{ produced})}{2 \times (\text{moles of EtOH fed})} \times 100$$

For ethylene steam reforming, all reaction parameters were kept identical except feeding 1.7% ethylene instead of 1.7% ethanol.

The quantitative analysis of the reactor effluents was carried out by online gas chromatography (Shimadzu Scientific 2010) equipped with a Carboxen column coupled with a pulsed discharge helium ionization detector (PDHID) which was used to separate and detect H_2, CO, and CO_2 and a Q-Bond column with a flame ionization detector (FID) to separate and detect the hydrocarbon species. The carbon balances were always better than 95%.

3. RESULTS AND DISCUSSION

3.1. Surface Area, Pore Volume, and XRD. The surface areas, pore volumes, and the average pore diameters of the ceria samples, with and without Co loading, are shown in Table 1.

Table 1. Surface Area and Pore Volume of CeO_2 and Co/CeO_2 Samples Measured Using N_2 Physisorption

	surface area m^2/g	pore volume cm^3/g	average pore diameter (Å)
CeO_2-MP	10	0.04	172
CeO_2-NP	120	0.12	39
Co/CeO_2-MP	8	0.03	170
Co/CeO_2-NP	34	0.04	40

The commercial ceria was found to have a significantly lower surface area of 10 m^2/g compared to the 120 m^2/g of the nanopolyhedra prepared by the solvothermal method. The average pore volumes of both samples were also significantly different with a lower average pore volume and larger average pore diameter for the CeO_2-MP sample.

Figure 1 shows the XRD patterns of the ceria samples where the most intense diffraction line is seen at a 2θ value of 28.5°,

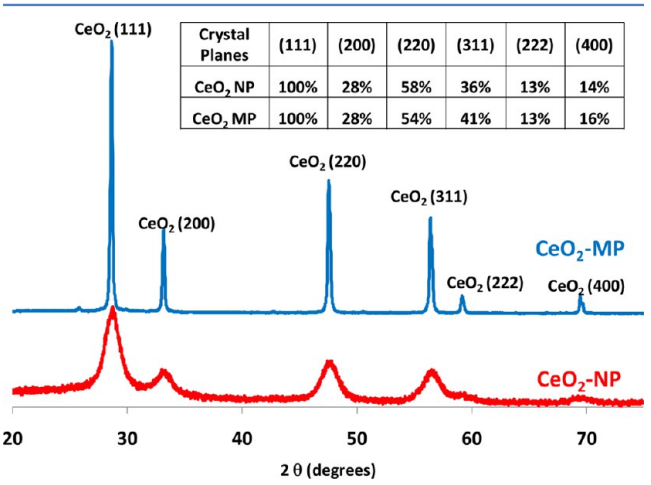

Figure 1. X-ray diffraction patterns of CeO_2-MP and CeO_2-NP. The inset shows the peak areas normalized with respect to the (111) diffraction line.

which indicates cerianite in the cubic phase (ICDD 81-792). The other diffraction lines at 33°, 47.5°, 56°, 59°, and 69.4° were identified as (200), (220), (311), (222), and (400) planes, respectively. Higher intensities and sharper peaks observed in the CeO_2-MP sample as opposed to the broader peaks in the CeO_2-NP pattern indicate higher crystallinity in the sample with the larger particle size. Scherrer calculations around the (111) peak have shown the particle size to be around 90 nm and 5 nm for CeO_2-MP and CeO_2-NP, respectively. The inset of Figure 1 tabulates the peak areas of the diffraction pattern, which are then normalized with respect to the (111) peak. Both samples show very similar distribution of crystal planes, which indicates similar morphologies for the two samples. Both the XRD patterns and the TEM images shown in the following section point to similar morphologies and allow us to assume that any possible effects of different crystal plane exposures or morphological differences, which are known to affect the catalytic behavior,[6,7,34] are negligible. This, in turn, allows isolating the effect of ceria particle size.

3.2. Transmission Electron Microscopy (TEM). Figure 2 shows digital micrographs of the CeO_2-MP and CeO_2-NP particles. Ceria particles prepared by the solvothermal method exhibited distinctly smaller particle sizes. The polyhedral morphologies of both samples were rather similar. Figure 3 shows the particle size distribution of the samples in a histogram where the average sizes were calculated to have a mean of 120 nm with a standard deviation of 50 nm (120 ± 50 nm) for the CeO_2-MP and 3.5 ± 1 nm for the CeO_2-NP. Analysis was done over a large sample area through multiple histograms to ascertain random sampling. The digital micrographs further establish the morphological similarities of both samples, allowing the focus of the study to be on the effect of particle size.

3.3. Temperature-Programmed Reduction (TPR). The ease of reducibility of the ceria samples was investigated using temperature programmed reduction. Fifty milligrams of CuO was used as a standard, and hydrogen required to reduce the sample was calculated to be 6.3×10^{-4} moles. Figure 4 shows the reduction profiles of both CeO_2-MP and CeO_2-NP. Although no significant reduction was observed below ~630

dx.doi.org/10.1021/cs400908h | ACS Catal. 2014, 4, 585−592

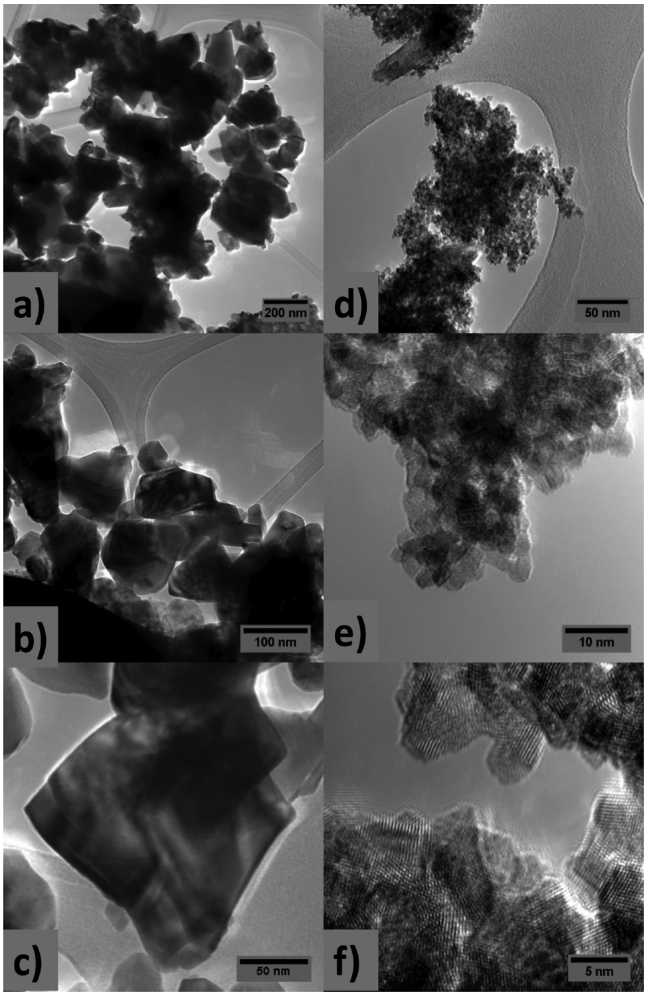

Figure 2. TEM images of (a, b, c) CeO_2-MP and (d, e, f) CeO_2-NP.

°C for the CeO_2-MP sample, the nanopolyhedra with a 3.5 nm average size were observed to reduce at much lower temperatures, with the maximum for H_2 consumption being around 390 °C. Assuming the $m/z = 2$ signal to be linear within the detection range, 50 mg of CeO_2-NP was observed to react with 3.2×10^{-5} moles of hydrogen, which corresponds to a stoichiometry of $CeO_{1.89}$. Laachir et al.[39] report approximately 20% Ce^{3+} and 80% Ce^{4+} at 700 K with a similar TPR analysis, which is consistent with 22% Ce^{3+} and 78% Ce^{4+} observed in our measurements. CeO_2-MP achieved the same degree of reduction at the much higher temperature of 750 °C. CeO_2-NP was observed to further reduce by reacting with an additional 1.7×10^{-5} moles of hydrogen to $CeO_{1.83}$, which corresponds to

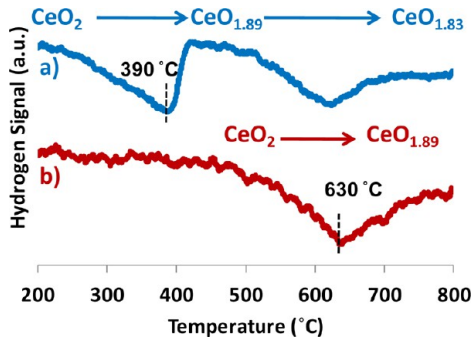

Figure 4. Temperature programmed reduction profiles of (a) CeO_2-NP and (b) CeO_2-MP.

34% Ce^{3+} and 66% Ce^{4+} at 700 °C . Ceria with the smaller particle size was found to be more readily reducible than the sample with a larger particle size. The oxidation state of the Ce is known to affect its acidic characteristics, with Ce^{3+} sites being significantly less acidic[43] than Ce^{4+}, thereby changing the surface chemistry. Further investigation of the reduction state of the ceria samples was conducted by *in situ* XANES.

3.4. X-Ray Adsorption near Edge Spectroscopy (XANES). The transformation of the cerium oxidation state during ethanol steam reforming for the preoxidized and prereduced nanopolyhedra was investigated by the XANES technique. Ceria samples with particle sizes larger than 25 nm were not observed to reduce below 600 °C. In situ XANES data for the CeO_2-NP in the 400−500 °C range are presented in Figure 5. Reference spectra for Ce^{3+} and Ce^{4+} are also included using $Ce(NO_3)_3$ and CeO_2 as standards, respectively. The insets show the 5.722−5.740 keV regions of the sample spectra only. The respective results of the linear combination fittings are presented in Table 2.

The oxidized sample was found to be in the form of CeO_2, whereas the reduced sample has shown 23% Ce^{3+}, which is in agreement with the TPR data presented in the previous section as well as the results of Laachir et al.[39] for similar reduction parameters. Although the starting oxidation states were quite different, both prereduced and preoxidized CeO_2-NP samples were found to converge to the same oxidation state and have a mixture of Ce^{3+} and Ce^{4+} oxidation states during steady-state ethanol steam reforming. Such behavior was previously reported in cobalt species in the ethanol steam reforming as well.[28,44,45] It should be noted that the reduction of cerium species was probed by predominantly bulk characterization techniques, and reported figures represent mainly bulk oxide ratios. Studies are underway to quantify the extent of surface reduction.

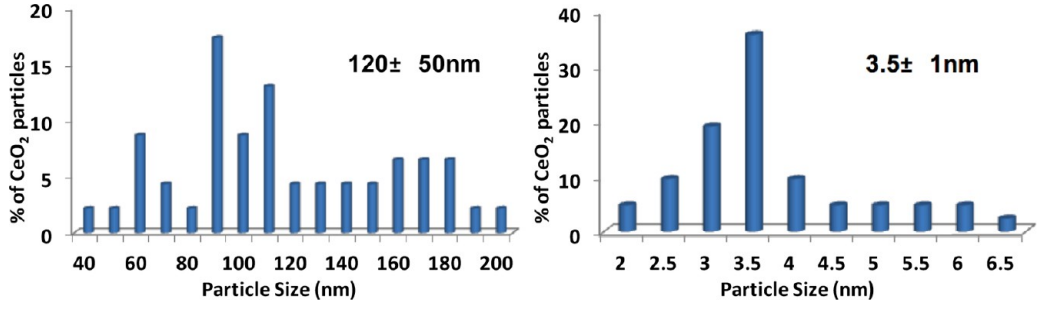

Figure 3. Particle size distribution histograms. (a) CeO_2-MP. (b) CeO_2-NP.

dx.doi.org/10.1021/cs400908h | *ACS Catal.* 2014, 4, 585−592

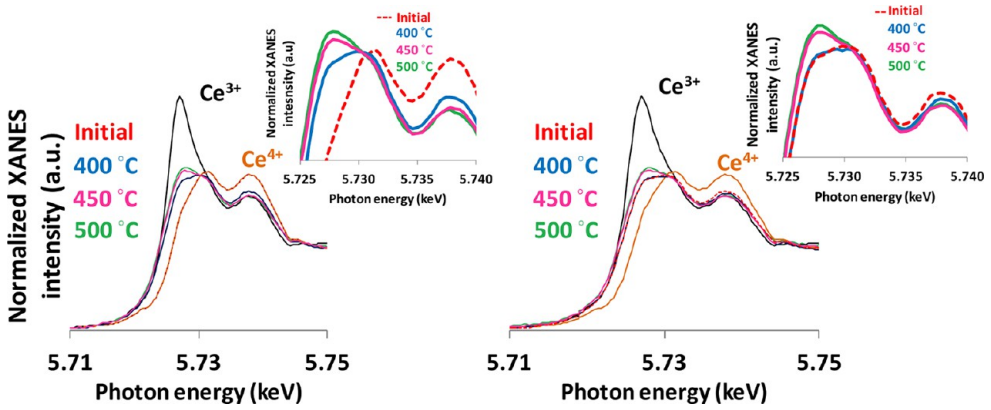

Figure 5. Operando XANES spectra for preoxidized (left) and prereduced (right) CeO_2-NP. Spectra for $Ce(NO_3)_3$ and CeO_2 are included as references for Ce^{3+} and Ce^{4+}, respectively. Insets: Enlarged views of the 5.722−5.740 keV regions for the sample spectra.

Table 2. Results of Linear Combination Fitting with Reference Compounds

	preoxidized		prereduced	
	$\%Ce^{3+}$	$\%Ce^{4+}$	$\%Ce^{3+}$	$\%Ce^{4+}$
after pretreatment		100	23	77
ESR at 400 °C	23	77	23	77
ESR at 450 °C	25	75	26	74
ESR at 500 °C	27	73	27	73

3.5. Diffuse Reflectance Infrared Spectroscopy (DRIFTS). DRIFTS studies focused on probing the catalyst surface for surface acidity and basicity. For Figures 6 and 7, the same detector gain and aperture sizes were used for both samples, which enabled comparison of the relative peak intensities.

Pyridine, being a basic molecule, was used to probe the acidic sites on CeO_2 samples. Figure 6 shows DRIFT spectra taken during pyridine temperature programmed desorption (TPD) in the 25−400 °C temperature range. The National Institute of Standards and Technology (NIST) chemistry webbook was used along with references 46−49 for identification of the vibrational energies. Upon room-temperature adsorption, bands to due molecularly adsorbed pyridine are apparent (C−C bonds at 1038, 1067, 116, 1147, and 1217 cm^{-1}; N−CH bond at 1284 cm^{-1}).[50] The band at 1441 could be due to molecularly adsorbed pyridine, but it could also represent a pyridinium species over a Bronsted acid site. Over the CeO2-NP sample, the only other major band seen at room temperature is the one at 1595 cm^{-1}, which can be assigned to H-bonded pyridine. All of the bands grow weaker with increasing temperature. Above 200 °C, however, three new bands appear, suggesting decomposition of pyridine. The band at 1564 cm^{-1} could be assigned to possibly acetates, and the ones at 1373 and 1354 cm^{-1} could be due to carbonates.[51] The spectra taken over this sample suggest a surface with a very low acidity.

The spectra taken over the CeO2-MP, on the other hand, present a much different picture. The bands due to molecular pyridine (1067, 1117, 1217, 1284 cm^{-1}) are also present in this sample. There are many more bands in the 1460−1420 range, suggesting pyridinium ions. The group of bands that is not well-resolved in the 1560−1480 cm^{-1} region may be due to pyridine adsorbed on Lewis acid sites. A band at 1595 cm^{-1} indicates the presence of H-bonded pyridine. Even at 400 °C, the bands at the Bronsted acid and Lewis acid regions are still very strong, although there is evidence of pyridine decomposition and conversion to acetates and carbonates as well, as seen through the bands at 1564, 1373, 1354, and 1313 cm^{-1}. The high intensity of these bands all indicates a highly acidic surface where pyridine adsorbs quite strongly.

CO_2, an acidic molecule, was used to probe for the basic sites by acquiring DRIFT spectra during CO_2 TPD. Figure 7 shows

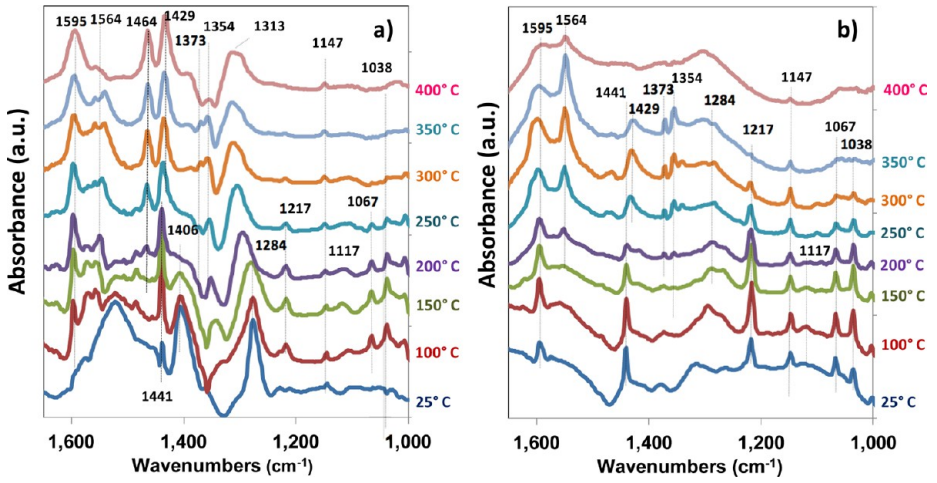

Figure 6. *In situ* DRIFT spectra during pyridine TPD. (a) CeO_2-MP. (b) CeO_2-NP. Samples were prereduced with H_2 prior to pyridine adsorption.

dx.doi.org/10.1021/cs400908h | ACS Catal. 2014, 4, 585−592

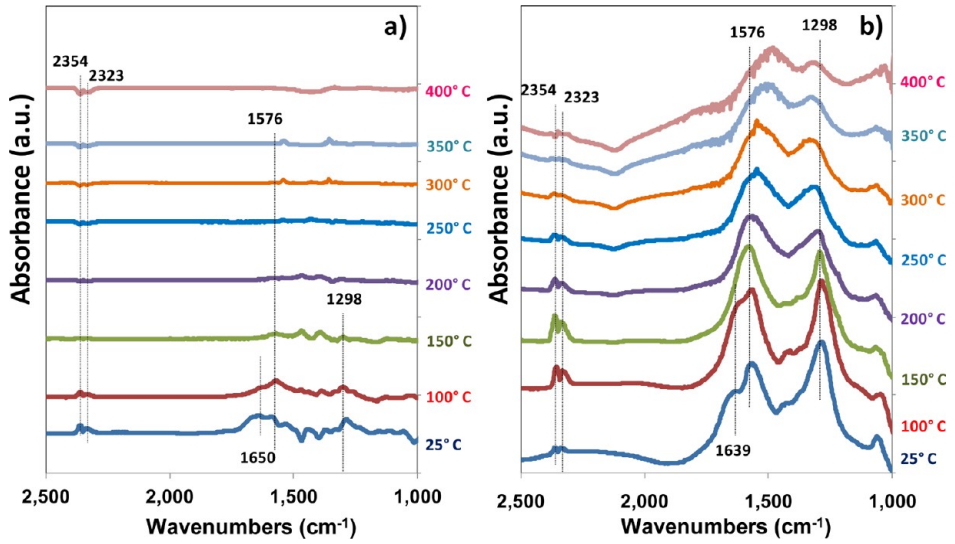

Figure 7. *In situ* DRIFT spectra during CO_2 TPD. (a) CeO_2-MP. (b) CeO_2-NP. Samples were prereduced with H_2 prior to CO_2 adsorption.

Table 3. Steady State Catalytic Activity Data for Steam Reforming of Ethanol over Oxidized and Pre-reduced CeO_2-MP CeO_2-NP Catalysts[a]

	350 °C				400 °C				450 °C			
products	MP(Ox)	MP(Red)	NP(Ox)	NP(Red)	MP(Ox)	MP(Red)	NP(Ox)	NP(Red)	MP(Ox)	MP(Red)	NP(Ox)	NP(Red)
% C_2H_5OH conversion	1.0	1.2	0.0	1.4	5.0	5.0	5.1	9.1	40.8	40.3	55.4	55.3
% H2 yield	0.4	0.5	0.0	1.0	2.0	2.2	1.6	2.9	12.0	12.6	15.3	15.3
% yield												
CO_2	0.5	0.6	0.0	1.1	2.4	2.3	1.8	2.7	12.1	12.8	14.9	15.0
CO	0.0	0.0	0.0	0.0	0.0	0.0	0.0	0.0	0.3	0.3	0.5	0.5
CH_4	0.0	0.0	0.0	0.0	0.0	0.0	0.1	0.1	0.4	0.4	0.9	1.1
C_2H_4	0.5	0.5	0.0	0.3	2.5	2.5	2.8	5.7	19.9	20.2	31.8	33.4
C_2H_6	0.0	0.0	0.0	0.0	0.0	0.0	0.2	0.1	0.1	0.1	1.5	1.5
CH_3COCH_3	0.0	0.0	0.0	0.0	0.0	0.0	0.0	0.0	6.6	6.7	2.0	3.1
CH_3CHO	0.0	0.0	0.0	0.0	0.0	0.0	0.0	0.0	0.0	0.0	0.8	0.8

[a] C_{EtOH} = 1.7% and H_2O/EtOH = 10:1 (molar ratio) 1 m^2 total surface area.

spectra collected for both samples, which have some bands in common, but diverge greatly in the relative intensities of the said bands. Moreover, the adsorbed species on CeO_2-MP do not persist beyond 150−200 °C. The major bands observed are at 1639, 1576, 1386, 1296, and 1049 cm^{-1}. The 1386 and 1049 cm^{-1} bands can be attributed to surface formates, which reform to carbonates as the temperature increases. The large bands around 1576 and 1290 cm^{-1} indicate ν_{as}(OCO) and ν_s(OCO), which can signal the presence of surface carbonates.[52,53] The band at 1639 cm^{-1} is likely due to adsorbed water. The CeO_2-NP sample has shown strong interaction with the adsorbed CO_2 throughout the temperature range, which can be explained by the presence of relatively more basic Ce^{3+} sites. The acidic probe persists even at 400 °C with the nanopolyhedra, whereas it was absent after 200 °C with the CeO_2-MP sample.

3.6. Steady-State Catalytic Activity Testing. *3.6.1. Ethanol Steam Reforming.* Steady-state activity testing over preoxidized (O) and prereduced (R) CeO_2-MP and CeO_2-NP catalysts was performed to investigate the effect of ceria particle size and the extent of reduction on steam reforming activity. Blank experiments with the same feed conditions showed no ethanol conversion within the temperature range of 350−450 °C, which indicated negligible gas phase reforming.

The products formed over both samples consisted of H_2, CO_2, CO, CH_4, C_2H_4, and C_2H_6 and the liquid products CH_3CHO and CH_3COCH_3. Equal surface area basis was used for the experiments where the catalyst loadings were varied to achieve 1 m^2 surface areas. Table 3 presents a comparison for ethanol conversion levels of hydrogen and carbon containing product yields between the two samples at 350, 400, and 450 °C. For each catalyst, two different pretreatment procedures are used. i.e., preoxidation or prereduction, as described earlier. The samples are not particularly active at 350 °C. At lower temperatures, the CeO_2-NP sample shows higher activity if it is prereduced. At 450 °C, the conversion and product distributions over this sample become very similar, regardless of the pretreatment used. As shown by the XANES data collected under steam reforming conditions (Figure 5), CeO_2-NP samples converge to the same cerium oxidation state under ethanol steam reforming conditions, hence leading to identical performances at higher temperatures.

CeO_2-MP samples, on the other hand, show very similar performances whether they were prereduced or not. These samples are never as active as the prereduced nanopolyhedra. This difference can be explained by the higher reducibility of the CeO_2-NP, and the higher activity of the Ce^{3+} sites. The sample with the larger particle size does not reduce during H_2-prereduction or under ethanol steam reforming conditions. Therefore, the pretreatment does not make any difference in the performance, leading to similar product distributions. The

dx.doi.org/10.1021/cs400908h | ACS Catal. 2014, 4, 585−592

prereduced CeO_2-NP samples outperform CeO_2-MP at every temperature.

The most prominent C-containing product over these catalysts is ethylene, reaching selectivity levels of ~50% for CeO_2-MP and ~60% for CeO_2-NP at 450 °C, suggesting that dehydration is a primary reaction pathway over ceria. Compared to ethylene, the other products, such as CH_4, CO and CH_3CHO are observed in much lesser quantities. However, over the CeO_2-MP sample, acetone is observed in substantial amounts, suggesting that ceria in its fully oxidized form can lead C−C bond formation, through ketonization reactions.[16,31]

Since ethylene was the primary product over these samples, they were further tested for ethylene steam reforming with C_2H_4 and H_2O in the reactant stream under the same feed conditions. Ceria, without any metal, did not show any catalytic activity for C−C bond cleavage. There was no detectable evidence of ethylene reforming or cracking, confirming that any ethylene that is formed from the dehydration of ethanol does not go through any further transformation over the ceria surfaces and is observed as a major product under steady-state conditions.

To test this assertion, the same ceria materials were impregnated with Co and used as catalysts in ethanol steam reforming, following a prereduction step. As expected, much higher conversions and H_2 yields were obtained as well as much higher CO_2 yields (Table 4). Some trends that were observed over the bare ceria samples appeared in this case as well, such as the substantial yield of acetone observed over the catalyst impregnated onto the CeO_2-MP support. These results indicate that, although cobalt is essential for C−C cleavage activity, the support may be contributing to the overall reaction network in significant ways.

Table 4. Steady State Catalytic Activity Data for Steam Reforming of Ethanol over Oxidized and Pre-reduced Co/CeO_2-MP Co/CeO_2-NP Catalysts[a]

	350 °C		400 °C		450 °C	
products	Co-MP	Co-NP	Co-MP	Co-NP	Co-MP	Co-NP
% C_2H_5OH conversion	16.4	20.9	44.0	40.2	81.3	97.1
% H2 yield	6.5	11.2	26.4	35.6	49.2	93.3
% yield						
CO_2	4.6	9.5	21.0	26.7	45.5	81.4
CO	0.0	0.0	0.3	0.0	0.6	0.0
CH_4	0.0	0.5	0.3	1.3	0.5	2.8
C_2H_4	0.2	0.2	2.5	2.1	8.4	4.7
C_2H_6	0.0	0.0	0.0	1.3	0.0	0.1
CH_3COCH_3	0.0	0.0	6.5	1.3	20.1	5.0
CH_3CHO	11.5	10.4	13.2	7.9	6.1	3.1

[a] C_{EtOH} = 1.7% and H_2O/EtOH = 10:1 (molar ratio) 1 m^2 total surface area.

4. CONCLUSIONS

Ceria samples with similar polyhedral morphologies but different particle sizes were investigated for their reducibility, surface acidity/basicity, and performance for ethanol and ethylene steam reforming in the absence of another metal or metal oxide. The ceria sample with the larger mean particle size of 120 nm had negligible reducibility below 600 °C. The nanopolyhedra with a mean particle size of 3.5 nm were found to reduce much more easily both with H_2 as well as during steady-state ethanol steam reforming, at temperatures as low as 400 °C. The presence of Ce^{3+} sites led to a less acidic surface over the 3.5 nm polyhedral sample. The differences in acidity manifested major differences in *in situ* DRIFTS spectra acquired during temperature-programmed desorption of probe molecules. In steady-state reaction experiments, ceria samples showed significant ethanol dehydration and steam reforming activity, with the more reduced samples exhibiting higher activity. No significant ethylene reforming was observed with either sample. Smaller particle size, increased reducibility and a higher surface density of the basic sites are thought to lead to higher activity for steam reforming. An important finding of the study is that ceria, which is commonly used as a support in many catalyst systems, has significant reducibility as well as catalytic activity in its own right and is likely to contribute to the observed activities of many catalysts supported on ceria.

AUTHOR INFORMATION

Corresponding Author

*Phone: 614-292-6623. Fax: 614-292-3769. E-mail: ozkan.1@osu.edu.

Notes

The authors declare no competing financial interest.

ACKNOWLEDGMENTS

We gratefully acknowledge the U.S. Department of Energy for the Grant DE-FG36-05GO15033 for our funding. XANES experiments were performed at the Dupont−Northwestern−Dow Collaborative Access Team (DND-CAT) located at Sector 5 of the Advanced Photon Source (APS). E.I. DuPont de Nemours & Co., The Dow Chemical Company, and the State of Illinois supported DND-CAT. Use of the APS was supported by the U.S. Department of Energy, Office of Science, Office of Basic Energy Sciences under Contract No. DE-ACO2-06CH11357. The authors acknowledge Hendrik E. Colijn for his invaluable help in taking and analyzing the digital micrographs.

REFERENCES

(1) Trovarelli, A. *Catal. Rev.: Sci. Eng.* **1996**, *38* (4), 439−520.
(2) Vivier, L.; Duprez, D. *ChemSusChem* **2010**, *3* (6), 654−678.
(3) Sayle, T. X. T.; Parker, S. C.; Sayle, D. C. *Phys. Chem. Chem. Phys.* **2005**, *7* (15), 2936−2941.
(4) Wu, Z.; Schwartz, V.; Li, M.; Rondinone, A. J.; Overbury, S. H. *J. Phys. Chem. Lett.* **2012**, *3*, 1517−1522.
(5) Xu, W. Q.; Liu, Z. Y.; Johnston-Peck, A. C.; Senanayake, S. D.; Zhou, G.; Stacchiola, D.; Stach, E. A.; Rodriguez, J. A. *ACS Catal.* **2013**, *3* (5), 975−984.
(6) Soykal, I. I.; Bayram, B.; Sohn, H.; Gawade, P.; Miller, J. T.; Ozkan, U. S. *Appl. Catal., A* **2012**, *449*, 47−58.
(7) Soykal, I. I.; Sohn, H.; Ozkan, U. S. *ACS Catal.* **2012**, *2* (11), 2335−2348.
(8) Breen, J. P.; Burch, R.; Coleman, H. M. *Appl. Catal., B* **2002**, *39* (1), 65−74.
(9) Rioche, C.; Kulkarni, S.; Meunier, F. C.; Breen, J. P.; Burch, R. *Appl. Catal., B* **2005**, *61* (1−2), 130−139.
(10) Kugai, J.; Velu, S.; Song, C. *Catal. Lett.* **2005**, *101* (3−4), 255−264.
(11) Kugai, J.; Subramani, V.; Song, C.; Engelhard, M. H.; Chin, Y.-H. *J. Catal.* **2006**, *238* (2), 430−440.
(12) Srinivas, D.; Satyanarayana, C. V. V; Potdar, H. S.; Ratnasamy, P. *Appl. Catal., A* **2003**, *246* (2), 323−334.

(13) Zhang, B.; Tang, X.; Li, Y.; Cai, W.; Xu, Y.; Shen, W. *Catal. Commun.* **2006**, *7* (6), 367−372.
(14) Song, H.; Ozkan, U. S. *J. Catal.* **2009**, *261* (1), 66−74.
(15) Song, H.; Ozkan, U. S. *J. Phys. Chem. A* **2010**, *114* (11), 3796−3801.
(16) Yee, A.; Morrison, S. J.; Idriss, H. *J. Catal.* **1999**, *186* (2), 279−295.
(17) Vaidya, P. D.; Rodrigues, A. E. *Chem. Eng. J. (Lausanne)* **2006**, *117* (1), 39−49.
(18) Haryanto, A.; Ferno, S.; Murali, N.; Adhikari, S. *Energy Fuels* **2005**, *19* (5), 2098−2106.
(19) Ni, M.; Leung, D. Y. C.; Leung, M. K. H. *Int. J. Hydrogen Energy* **2007**, *32* (15), 3238−3247.
(20) Mattos, L. V.; Jacobs, G.; Davis, B. H.; Noronha, F. B. *Chem. Rev.* **2012**, *112*, 4094−4123.
(21) Bshish, A.; Yaakob, Z.; Narayanan, B.; Ramakrishnan, R.; Ebshish, A. *Chem. Pap.* **2011**, *65* (3), 251−266.
(22) Song, H.; Bao, X.; Hadad, C. M.; Ozkan, U. S. *Catal. Lett.* **2011**, *141* (1), 43−54.
(23) Song, H.; Mirkelamoglu, B.; Ozkan, U. S. *Appl. Catal., A* **2010**, *382* (1), 58−64.
(24) Song, H.; Ozkan, U. S. *J. Mol. Catal. A: Chem* **2010**, *318* (1−2), 21−29.
(25) Song, H.; Tan, B.; Ozkan, U. S. *Catal. Lett.* **2009**, *132* (3−4), 422−429.
(26) Song, H.; Zhang, L.; Ozkan, U. S. *Ind. Eng. Chem. Res.* **2010**, *49* (19), 8984−8989.
(27) Song, H.; Zhang, L.; Ozkan, U. S. *Top. Catal.* **2012**, *55* (19−20), 1324−1331.
(28) Bayram, B.; Soykal, I. I.; von Deak, D.; Miller, J. T.; Ozkan, U. S. *J. Catal.* **2011**, *284* (1), 77−89.
(29) Calaza, F. C.; Xu, Y.; Mullins, D. R.; Overbury, S. H. *J. Am. Chem. Soc.* **2012**, *134*, 18034−18045.
(30) Wu, Z.; Li, M.; Schwartz, V.; Overbury, S. H. In *Shape Effect in Metal Oxide Catalysis: Ceria Nanoshapes As Catalysts and Supports*; American Chemical Society: Washington, DC, 2013; pp CATL−96.
(31) Gangadharan, A.; Shen, M.; Sooknoi, T.; Resasco, D. E.; Mallinson, R. G. *Appl. Catal., A* **2010**, *385* (1−2), 80−91.
(32) Noronha, F. B.; Fendley, E. C.; Soares, R. R.; Alvarez, W. E.; Resasco, D. E. *Chem. Eng. J. (Lausanne)* **2001**, *82* (1−3), 21−31.
(33) Noronha, F. B.; Shamsi, A.; Taylor, C.; Fendley, E. C.; Stagg-Williams, S.; Resasco, D. E. *Catal. Lett.* **2003**, *90* (1−2), 13−21.
(34) Si, R.; Flytzani-Stephanopoulos, M. *Angew. Chem., Int. Ed.* **2008**, *47* (15), 2884−2887.
(35) Yi, N.; Si, R.; Saltsburg, H.; Flytzani-Stephanopoulos, M. *Energy Environ. Sci.* **2010**, *3* (6), 831−837.
(36) Yi, N.; Si, R.; Saltsburg, H.; Flytzani-Stephanopoulos, M. *Appl. Catal., B* **2010**, *95* (1−2), 87−92.
(37) Boucher, M. B.; Goergen, S.; Yi, N.; Flytzani-Stephanopoulos, M. *Phys. Chem. Chem. Phys.* **2011**, *13* (7), 2517−2527.
(38) Zhou, X. D.; Huebner, W. *Appl. Phys. Lett.* **2001**, *79* (21), 3512−3514.
(39) Laachir, A.; Perrichon, V.; Badri, A.; Lamotte, J.; Catherine, E.; Lavalley, J. C.; El Fallah, J.; Hilaire, L.; Le Normand, F.; Quemere, E.; Sauvion, G. N.; Touret, O. *J. Chem. Soc., Faraday Trans.* **1991**, *87* (10), 1601−1609.
(40) Nolan, M.; Grigoleit, S.; Sayle, D. C.; Parker, S. C.; Watson, G. W. *Surf. Sci.* **2005**, *576* (1−3), 217−229.
(41) Nolan, M. *J. Mater. Chem.* **2011**, *21* (25), 9160−9168.
(42) Zhou, K.; Wang, X.; Sun, X.; Peng, Q.; Li, Y. *J. Catal.* **2005**, *229* (1), 206−212.
(43) Patnaik, P. *Handbook of Inorganic Chemicals* **2003**, 199−200.
(44) Lin, S. S. Y.; Kim, D. H.; Ha, S. Y. *Catal. Lett.* **2008**, *122* (3−4), 295−301.
(45) Lin, S. S. Y.; Kim, D. H.; Ha, S. Y. *Appl. Catal., A* **2009**, *355* (1−2), 69−77.
(46) Zaiku, X.; Qingling, C.; Chengfang, Z.; Jiaqing, B.; Yuhua, C. *J. Phys. Chem. B* **2000**, *104* (13), 2853−2859.
(47) Zhu, X.; Liu, S.; Song, Y.; Xu, L. *Catal. Commun.* **2005**, *6* (11), 742−746.
(48) Zhang, J.; Chen, J.; Ren, J.; Sun, Y. *Appl. Catal., A* **2003**, *243* (1), 121−133.
(49) Llorca, J.; Homs, N.; Ramirez de la Piscina, P. *J. Catal.* **2004**, *227* (2), 556−560.
(50) Perelygin, I. S.; Klimchuk, M. A. *J. Appl. Spectrosc.* **1976**, *24* (1), 43−46.
(51) Zaki, M. I.; Hussein, G. A. M.; Mansour, S. A. A.; El-Ammawy, H. A. *J. Mol. Catal.* **1989**, *51* (2), 209−220.
(52) Bollinger, M. A.; Vannice, M. A. *Appl. Catal., B* **1996**, *8* (4), 417−443.
(53) Jacobs, G.; Williams, L.; Graham, U.; Thomas, G. A.; Sparks, D. E.; Davis, B. H. *Appl. Catal., A* **2003**, *252* (1), 107−118.